Prediction of Parachute Line Sail During Lines-First Deployment

James W. Purvis*
Sandia National Laboratories, Albuquerque, New Mexico

A numerical deployment simulation with the capability to predict line sail is presented. A finite-element approach is used in which both canopy and suspension lines are modeled as flexible, distributed-mass structures connected to a finite-mass forebody. The model includes all aspects of the deployment problem, such as suspension line aerodynamics, line ties, and canopy/deployment bag friction. The model has been verified by comparison with experimental data and used to investigate proposed solutions for a system with a line sail problem.

Nomenclature

A_i = cross-sectional area of suspension line at ith node, ft^2
a_∞ = speed of sound, ft/s
B_i = tensile damping coefficient at ith node, lb-s
B_0 = tensile damping constant, s^{-1}
C_A = tangential aerodynamics force coefficient
C_D = drag coefficient
C_{N_α} = aerodynamic normal force coefficient derivative
E_i = elastic modulus of ith node, psf
$f(M_\infty)$ = viscous cross flow normal force derivative
F_{N_i}, F_{A_i} = aerodynamic forces at ith node, lb
F_{x_i}, F_{r_i} = axial and radial forces at ith node, lb
K_{LG} = line group interference factor
K_T = line twist factor
m_i = mass of ith node, slugs
N = number of suspension lines
q = dynamic pressure, psf
S = aerodynamic coefficient reference area, ft^2
s_i = distance between nodes i and $i+1$, ft
s_L = suspension line length, ft
s_{0_i} = unstretched distance between nodes i and $i+1$, ft
T_i = tension in ith line segment, lb
V_i = total speed of ith node, ft/s
V_{T_i} = tangential velocity component at node i, ft/s
w = suspension line width, ft
x,r = cylindrical coordinates
α_i = aerodynamic angle of attack of ith line segment
ϵ_i = strain of ith line segment
ρ_i = material density at node i, slugs/ft^3
ρ_∞ = ambient air density, slugs/ft^3
μ_∞ = ambient air viscosity, slugs/ft-s
θ_i = line segment orientation angle

Introduction

ON December 16, 1981, a 2400 lb store, 18 in. in diameter and 12 ft long was released from an F-111 bomb bay at Mach 1.28. Aircraft flowfield interference caused the store to exit the bomb bay at approximately 20 deg angle of attack. The store contained a decelerator system consisting of a 46-ft-diam ribbon parachute with 50-ft suspension lines. Due to the high angle of attack and high dynamic pressure, the decelerator system experienced severe line sail, which, in turn, contributed to a bad canopy deployment and inflation, and an undesirably high impact velocity. The severity of the line sail at line stretch is illustrated in Fig. 1, which contains two successive frames of high-speed film of the test. The looping of the lines over and past the deployment bag is readily apparent.

The phenomenon of line sail (also known as "fish hooking") and its predecessor, line bowing, generally occurs during a deployment in which the relative wind is not parallel to the deployment direction. Both line bowing and line sail have been known to cause or contribute to the following problems: increased deployment times, changes in snatch load, asymmetrical deployment, friction damage, and unpredictable canopy inflation. The mechanisms for controlling line sail are pilot parachute drag area, line tie numbers and strengths, and deployment bag design.

The cut-and-try test procedure, generally employed to solve problems such as that described above, is both expensive and time-consuming. Consequently, analytical methods of investigating proposed solutions are highly desirable. Unfortunately, most analytical deployment schemes are similar to those presented in Ref. 1, and have no capability for modeling line sail. French[2] developed analytical solutions for

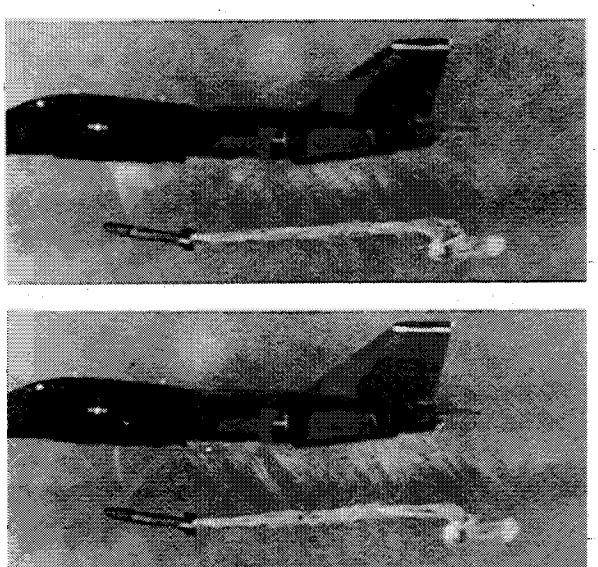

Fig. 1 Flight test deployment with severe line sail, Mach 1.28.

Submitted Sept. 9, 1982; revision received May 9, 1983. This paper is declared a work of the U.S. Government and therefore is in the public domain.

*Member of Technical Staff, Aerodynamics Department 1630. Member AIAA.

the effect of line ties on deployment time and velocity; however, his model was restricted to either constant forebody velocity or acceleration, and had no line sail modeling. Discrete element deployment schemes such as Refs. 3 and 4 are conceptually the most promising methods, although only Moog[5] appears to have addressed the line bowing problem per se. Moog's model produced good correlation between predicted line bowing and low q flight test data, even though the entire suspension line/canopy system was modeled as only three mass points. As noted in his conclusions, this was an insufficient number to accurately model the problem, and led to some unrealistic behavior such as "twanging" as a lumped mass was deployed from the bag. Line tie effects were also difficult to estimate, as was line sail.

The objective of the present work is to develop a numerical deployment simulation with the capability to accurately predict line sail. The method uses a finite-element approach similar to that of Sundberg[4] in which both canopy and suspension lines are modeled as flexible, distributed-mass structures connected to a finite-mass forebody. The line segments are sequentially deployed from the deployment bag, and their motion is determined by line tie and aerodynamic forces as well as line tension. Both normal and tangential aerodynamic forces are accounted for, including the effects of line grouping and line twist, and extraction of the deployment bag from the forebody is also modeled. Accuracy of the various aspects of the simulation is determined by comparison with experimental data. The method is shown to accurately predict line sail for the F-111 case previously described.

Analysis

The physical system and a schematic representation of the discrete element model are shown in Fig. 2. The forebody, suspension lines, canopy, and pilot parachute/deployment bag are modeled as a series of elastically connected mass nodes. The motion of each node is determined by the tensile and aerodynamic forces acting on the structural segment represented by the node. The forebody and pilot parachute/deployment bag are separate special nodes, with all undeployed suspension line or canopy nodes lumped in the pilot parachute/deployment bag node. The aerodynamic forces on the forebody and pilot parachute/deployment bag nodes consist of forebody drag and pilot parachute drag, respectively.

Referring to Fig. 3, the equations of motion for the ith deployed mass node are

$$m_i\ddot{x}_i = T_i\cos\theta_i - T_{i-1}\cos\theta_{i-1} + F_{x_i} \tag{1a}$$

$$m_i\ddot{r}_i = T_i\sin\theta_i - T_{i-1}\sin\theta_{i-1} + F_{r_i} \tag{1b}$$

where T_i is the tension between nodes i and $i+1$, and F_x, F_r are the axial and radial components of the aerodynamic forces acting on the line segment represented by the ith node.

Following Moog,[5] the tension between two mass nodes is expressed as a low strain rate stress-strain relation plus a linear damping term

$$T_i = E_iA_iN\epsilon_i + B_i\dot{\epsilon}_i \tag{2}$$

The strain and strain rate are computed from

$$\epsilon_i = (s_i - s_{0_i})/S_{0_i} \tag{3a}$$

and

$$\dot{\epsilon}_i = \dot{s}_i/s_{0_i} \tag{3b}$$

Negative values of tension are not allowed. From the geometry of Fig. 4, the line segment length is

$$s_i = \sqrt{(x_{i+1}-x_i)^2 + (r_{i+1}-r_i)^2} \tag{4a}$$

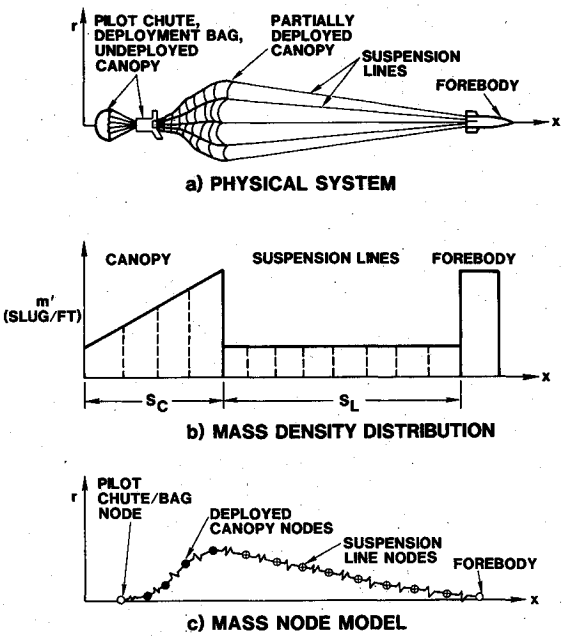

Fig. 2 Discrete element model.

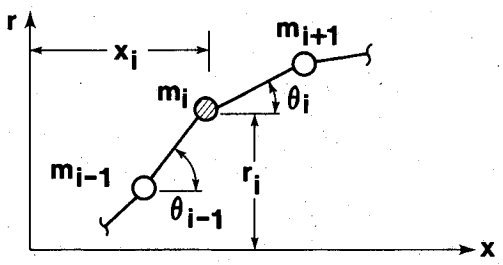

Fig. 3 Mass node geometric parameters.

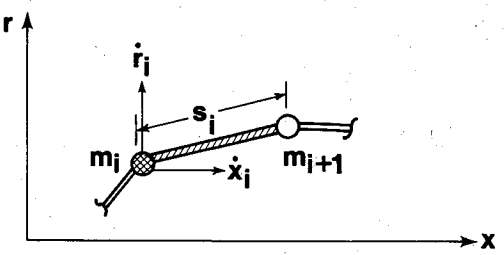

Fig. 4 Line segment tension parameters.

Differentiation gives

$$\dot{s}_i = [(x_{i+1}-x_i)(\dot{x}_{i+1}-\dot{x}_i) + (r_{i+1}-r_i)(\dot{r}_{i+1}-\dot{r}_i)]/s_i \tag{4b}$$

The elastic modulus E_i is computed using the linear stress-strain assumption[4] and rated strength vs elongation-at-failure data

$$E_i = \text{rated strength}/A_i\epsilon_{\max} \tag{5}$$

The damping parameter B_i is

$$B_i = 2B_0m_i\sqrt{E_i/\rho_i} \tag{6}$$

where E_i/ρ_i is the wavespeed in the line material and the constant B_0 has a value between 0 for no damping and ½ for critical damping. The form of the damping parameter was determined analytically from the longitudinal equation of motion of a single line segment fixed at one end and given an initial unit displacement at the other. The constant B_0 was

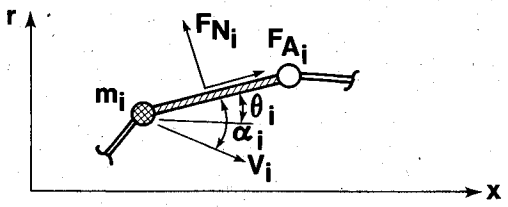

Fig. 5 Line segment aerodynamic forces.

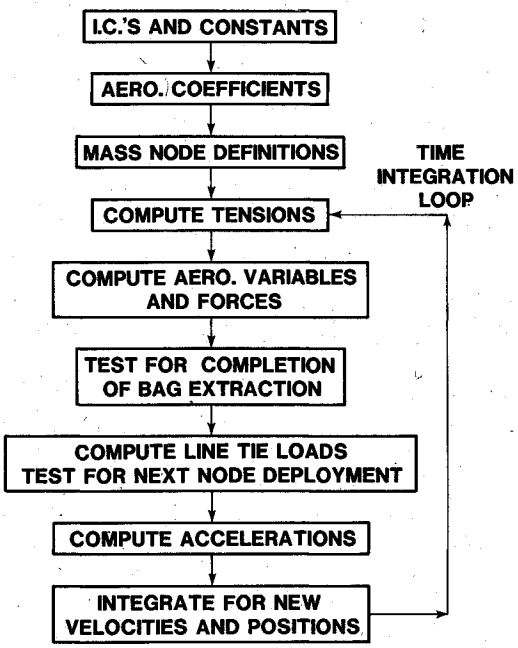

Fig. 6 Deployment simulation program flow.

determined by numerical experiment, and was found to be 85% of that required for critical damping (Moog[5] recommended using 5-10%). The large value was required in part by the one-step Euler integration scheme used in the present analysis.

The axial and radial components of the line segment aerodynamic forces, shown in Fig. 5, are:

$$F_{x_i} = -F_{N_i}\sin\theta_i + F_{A_i}\cos\theta_i \tag{7a}$$

$$F_{r_i} = F_{N_i}\cos\theta_i + F_{A_i}\sin\theta_i \tag{7b}$$

The expression for the normal force is similar to that used by Sundberg,[4] which is based on the familiar cross flow-drag formulations (see, for example, Ref. 6)

$$F_{N_i} = (NK_TK_{LG})\,qSC_N\sin\alpha_i\,|\sin\alpha_i| \tag{8}$$

The dynamic pressure, q, and angle of attack, α_i, in Eq. (8) are based on the speed orientation of the ith node with respect to the absolute velocity vector. The dynamic pressure q has the usual form based on the square of the node velocity. The node reference area, which is an individual line segment planform area, is

$$S = ws_{0_i} \tag{9}$$

where w is the suspension line width and s_{0_i} is the unstretched length of the element. The normal force coefficient derivative is

$$C_{N_\alpha} = f(M_\infty) \tag{10}$$

Since the suspension lines for the systems of interest in the current work are flat ribbons, the aerodynamic normal force due to cross flow on an isolated ribbon segment should be the same as that on a two-dimensional flat plate. However, during deployment the lines are bunched together forming a rough cylinder with a diameter equal to the deployment bag diameter. The net aerodynamic normal force due to cross flow on the line segment bunch should then be approximately the same as that on a two-dimensional circular cylinder. To model both behaviors, the form of the function $f(M_\infty)$ was taken from viscous cross-flow effects on a circular cylinder,[6] with the magnitude adjusted such that the zero Mach value corresponds to the two-dimensional incompressible flat plate drag coefficient. The behavior of the function in the critical Reynolds number regime was found to be important.

The net normal force on a node is reduced by the product of a line twist factor K_T and a line group factor K_{LG}. The line twist factor represents a reduction in the actual load on a line segment due to the fact that the line segment may be twisted. When the line segment is twisted, the cross-flow velocity component is no longer perpendicular to the maximum planform area of the segment. The actual cross-flow velocity component normal to the planform is the net cross-flow component reduced by the cosine of the twist angle. Assuming that each line segment has a specific twist angle, and that the distribution of twist angles is uniform between 0 and π, then the twist factor may be expressed as

$$K_T = \left(\frac{2}{N}\right)\sum_{i=1}^{N/2}\cos\left(\frac{\pi i}{N}\right) \tag{11}$$

where N is the total number of lines. The summation must be evaluated numerically.

Similarly, the line group factor (sometimes known as the shadow factor) accounts for the shielding of some lines in the group from the cross-flow velocity by other segments which are upwind. Assuming a uniform distribution in load between zero and the maximum, the line group factor may be expressed as

$$K_{LG} = \frac{1}{N}\sum_{i=1}^{N}\left(\frac{i}{N}\right) = \frac{N+1}{2N} \tag{12}$$

The axial (tangential) aerodynamic load on a line segment is assumed to consist solely of a turbulent skin-friction drag acting on the wetted area of each segment. The form of the tangential force is

$$F_{A_i} = -\tfrac{1}{2}\rho_\infty V_{T_i}|V_{T_i}|N(2S)C_A \tag{13}$$

where the negative sign and the absolute value are used to give the proper direction to the force. The factor of two in front of the area accounts for the fact that the wetted area is twice the planform area of a line segment. The axial force coefficient, given by

$$C_A = 0.37/[\rho_\infty a_\infty s_L/\mu_\infty]^{0.2} \tag{14}$$

is based on an approximate turbulent skin-friction drag formula derived from an experiment by Blasius.[7] The formula is based on freestream speed of sound and suspension line length rather than line segment velocity and length; however, the magnitude is still small, and experimental data[7] show that the turbulent skin-friction coefficient for a flat plate varies less than 10% for Mach numbers up to 2.

The effects of line ties and deployment bag friction, where appropriate, are incorporated into the tension or force equations, respectively. Line tie effects are represented as a node deployment restriction. Untied nodes are allowed to deploy only when two conditions are met: 1) the previous node has been deployed, and 2) a nonzero tension exists in the line segment between the deployed and undeployed nodes. When a node is tied, the second condition is modified such

that the tension in the segment must be greater than the rated strength of the ties before the node is allowed to deploy.

As noted by Moog,[5] the magnitude of the deployment bag friction force, also known as inelastic bag stripping force, is commonly determined in ground tests. In the present analysis, bag friction is represented as a constant force acting only on the last deployed node. The force is assumed to act on the node from the time it is deployed until the next successive node is deployed. The line of action of the force is along the segment between the last deployed node and the deployment bag node.

Results

The deployment simulation program flow, which incorporates the complete analysis, is shown in Fig. 6. Prior to any attempt at predicting line sail, various aspects of the simulation were studied and compared with experiment. In addition, values for driving parameters, such as canopy/deployment bag friction and pilot parachute drag area, had to be obtained from experimental data.

First, the dynamics equations (1-4) were verified by comparison with data from a static deployment test.[8] In the static test, a 20-ft-diam parachute system was ejected at 190 ft/s from the forebody by means of a gas piston arrangement. The momentum of the parachute pack was then used to deploy the suspension lines and canopy. No aerodynamics were involved since the forebody was rigidly fixed in a test stand.

Figures 7 and 8 compare various simulation results with displacement and separation velocity data for the system. The simulation equations, with 30 mass nodes for the lines and 20 for the canopy, produced smooth, well-behaved results. Simulation results with and without line ties were identical, indicating that the effect of line ties on the deployment was negligible. The separation velocity data indicated that a constant internal friction force acted during canopy deployment, since the separation velocity remained constant during line deployment but decreased linearly during canopy deployment. The magnitude of this friction force was determined by numerical experiment. Successive simulation runs were made, each with a different, constant value of friction force acting during canopy deployment. As shown in Figs. 7 and 8, the best data comparison (the "with friction" theory) was achieved when the magnitude of the friction force was fixed at 1700 lb.

Next, drag area C_DS vs Mach number was determined for the 5-ft-diam ribbon pilot parachute used to deploy the system mentioned in the Introduction. The drag area was determined by iteration and comparison with data for horizontal deployments in which the freestream flow remained aligned with the deployment direction. The iteration process consisted of the following steps: 1) assume a constant value of C_DS for the pilot parachute during deployment; 2) compare deployment simulation results with separation vs time data; and 3) change C_DS and repeat the first two steps until the best overall match with data is obtained.

Sample results are shown in Figs. 9 and 10, where the pilot parachute was used to deploy a 40-ft-diam main canopy with 50-ft suspension lines.[9] The forebody velocity was Mach 1.24. The iteration procedure and similar comparisons at other Mach numbers were used to produce a C_DS vs M_∞ curve for the pilot parachute.

Finally, the complete model was used to simulate the test described in the Introduction in which severe line sail was encountered.[10] In the test, a 46-ft-diam main canopy with 50-

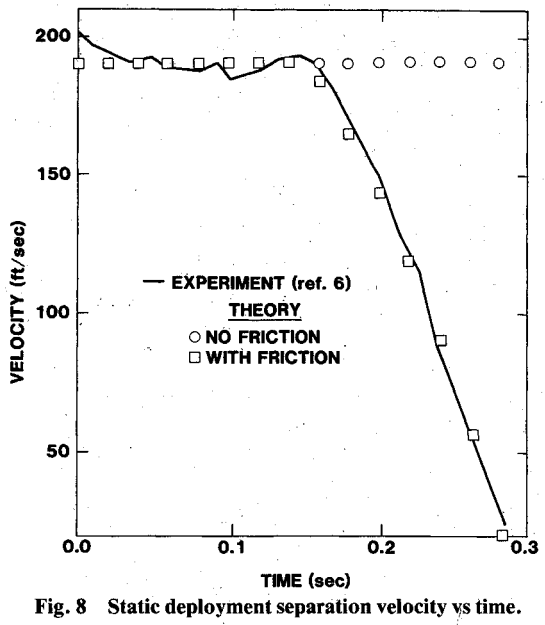

Fig. 8 Static deployment separation velocity vs time.

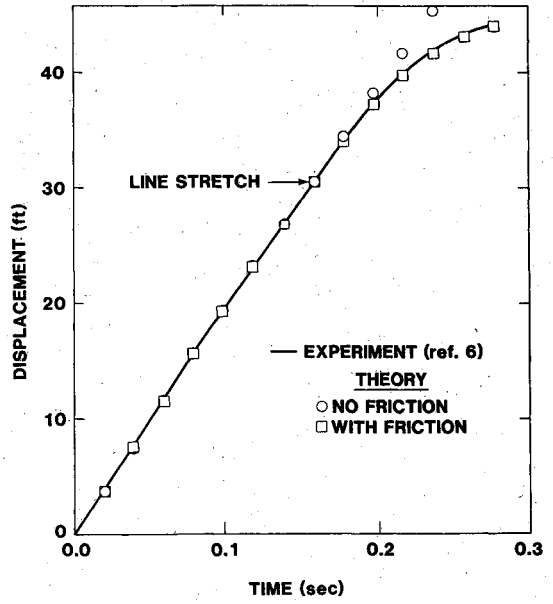

Fig. 7 Static deployment displacement vs time.

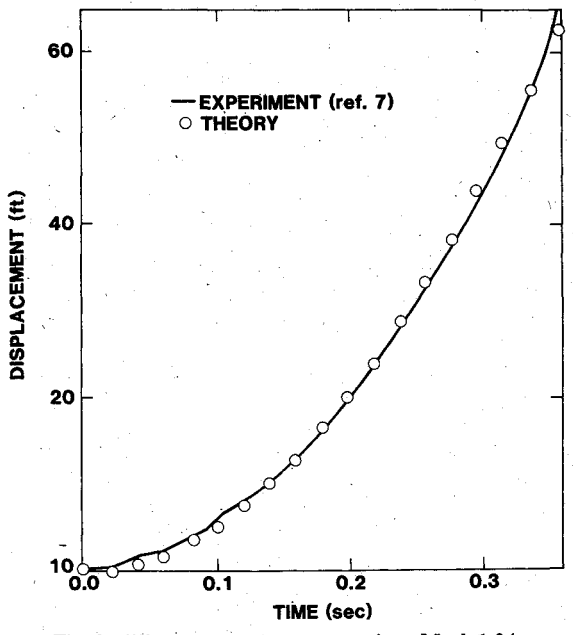

Fig. 9 Flight test displacement vs time, Mach 1.24.

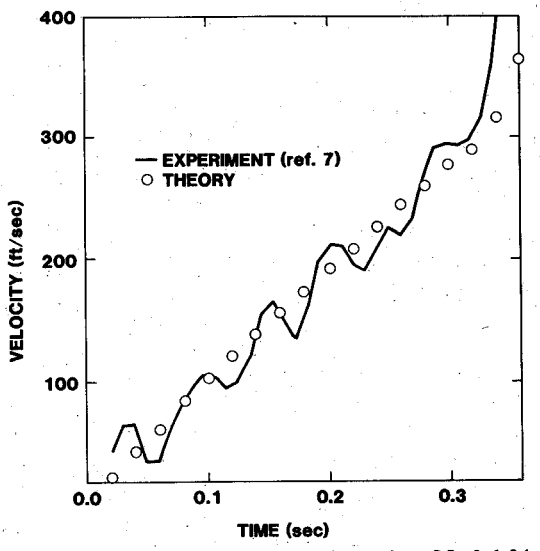

Fig. 10 Flight test separation velocity vs time, Mach 1.24.

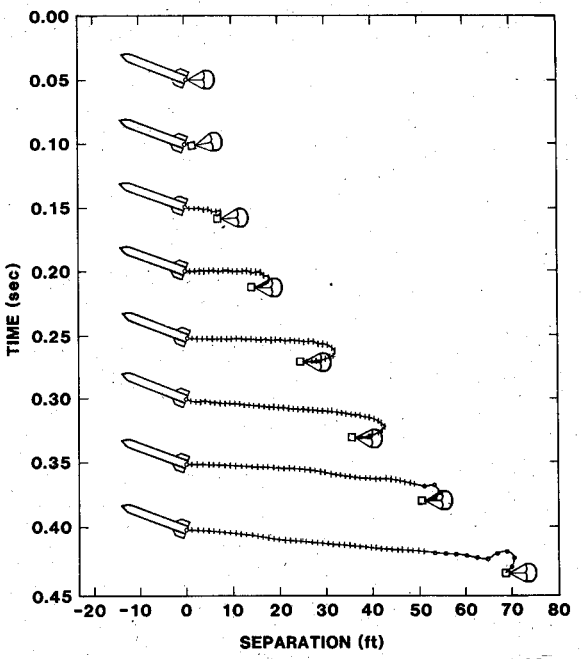

Fig. 11 Predicted high α deployment history, Mach 1.28.

ft suspension lines was deployed at Mach 1.28 from a forebody at 20 deg angle of attack. Line ties and previously determined pilot parachute drag areas were incorporated in the simulation. Since the pack densities of the present system and the previously discussed static ejection system were similar, a 1700 lb canopy/deployment bag friction force was assumed to act on canopy nodes during deployment. No attempt was made to model or otherwise account for canopy inflation during deployment.

A time history of the deployment is shown in Fig. 11, where the "+" symbols represent suspension line mass nodes and the circles are canopy nodes. The computer graphics depiction of the line sail was found to correlate extremely well with high-speed film of the tests. As a qualitative comparison, the simulation results at 0.30 s in Fig. 11 correspond to the frames from the flight test shown in Fig. 1. Simulation results for the time-to-line stretch and canopy stretch were 0.29 and 0.40 s, respectively, which also agreed very well with the measured values of 0.33 ± 0.02 and 0.41 ± 0.02 s from the test.

Subsequent simulation results indicated that practical changes in the line tie strengths could not control or eliminate

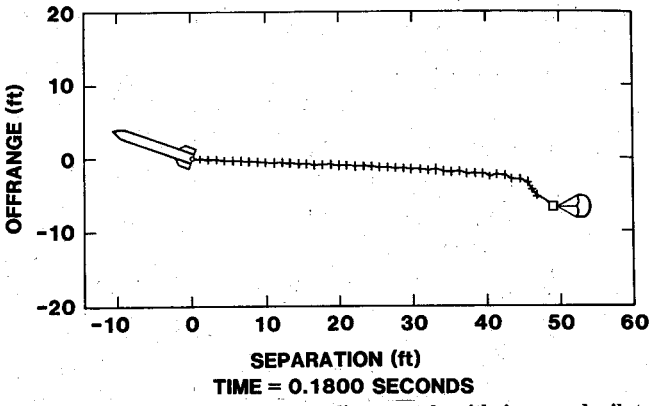

Fig. 12 Predicted deployment at line stretch with increased pilot parachute drag area, Mach 1.28.

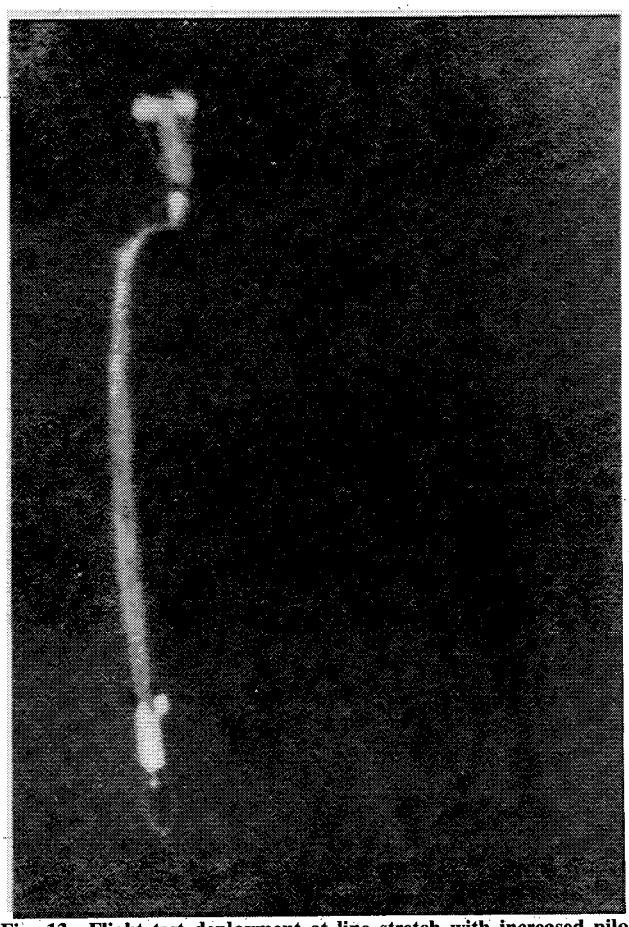

Fig. 13 Flight test deployment at line stretch with increased pilot parachute drag area, Mach 1.28.

the line sail. The simulation was then used to resize the pilot parachute system of Ref. 10. An example is shown in Fig. 12, where the pilot parachute drag area was increased by a factor of 4, resulting in a 40% decrease in time-to-line stretch with no line sail and only a small amount of line bowing. Figure 13, which corresponds to the simulation prediction in Fig. 12, is a sample of the subsequent flight test results using the new pilot parachute system.

Conclusions

A numerical deployment simulation has been developed with the capability of accurately predicting line sail. The model includes all aspects of the deployment problem, such as suspension line aerodynamics, line tie effects, and canopy/deployment bag friction. The model has been verified

by comparison with experimental data, and used to investigate a solution for a system with a line sail problem. The major cause of line sail was determined to be the relative magnitude of suspension line aerodynamic forces and pilot parachute drag when the freestream flow is not aligned with the deployment direction.

Acknowledgment

This work was supported by the U.S. Department of Energy.

References

[1]McVey, D. F. and Wolf, D. F., "Analysis of Deployment and Inflation of Large Ribbon Parachutes," *Journal of Aircraft*, Vol. 11, Feb. 1972, pp. 96-103.

[2]French, K. E., "Effects of Line Ties on Parachute Deployment," *Journal of Spacecraft and Rockets*, Vol. 17, May-June 1980, pp. 260-262.

[3]Keck, E. L., "A Computer Simulation of Parachute Opening Dynamics," AIAA Paper 75-1379, Albuquerque, N. Mex., Nov. 1975.

[4]Sundberg, W. D., "Finite-Element Modeling of Parachute Deployment and Inflation," AIAA Paper 75-1380, Albuquerque, N. Mex., Nov. 1975.

[5]Moog, R. D., "Aerodynamic Line Bowing During Parachute Deployment," AIAA Paper 75-1381, Albuquerque, N. Mex., Nov. 1975.

[6]Jorgensen, L. H., "Prediction of Static Aerodynamic Characteristics for Slender Bodies Alone and with Lifting Surfaces to Very High Angles of Attack," NASA TR R-474, Calif., Sept. 1977.

[7]Kuethe, A. M. and Schetzer, J. D., *Foundations of Aerodynamics*, John Wiley and Sons, New York, pp. 315-324.

[8]C de Baca, J. E., "Optical Reduction on Test R714002," unclassified internal memorandum, Sandia National Labs., Albuquerque, New Mex., Sept. 16, 1976.

[9]Simpson, S. L., "Data Reduction Report, Sandia Test R722005," Tonopah Test Range, Sandia National Labs., Albuquerque, N. Mex., Dec. 16, 1981.

[10]Silva, P. D., "Data Reduction Report, Sandia Test R722014," Tonopah Test Range, Sandia National Labs., Albuquerque, N. Mex., Dec. 16, 1981.

From the AIAA Progress in Astronautics and Aeronautics Series..

EXPERIMENTAL DIAGNOSTICS IN COMBUSTION OF SOLIDS—v. 63

Edited by Thomas L. Boggs, Naval Weapons Center, and Ben T. Zinn, Georgia Institute of Technology

The present volume was prepared as a sequel to Volume 53, *Experimental Diagnostics in Gas Phase Combustion Systems*, published in 1977. Its objective is similar to that of the gas phase combustion volume, namely, to assemble in one place a set of advanced expository treatments of the newest diagnostic methods that have emerged in recent years in experemental combustion research in heterogenous systems and to analyze both the potentials and the shortcomings in ways that would suggest directions for future development. The emphasis in the first volume was on homogenous gas phase systems, usually the subject of idealized laboratory researches; the emphasis in the present volume is on heterogenous two- or more-phase systems typical of those encountered in practical combustors.

As remarked in the 1977 volume, the particular diagnostic methods selected for presentation were largely undeveloped a decade ago. However, these more powerful methods now make possible a deeper and much more detailed understanding of the complex processes in combustion than we had thought feasible at that time.

Like the previous one, this volume was planned as a means to disseminate the techniques hitherto known only to specialists to the much broader community of reesearch scientists and development engineers in the combustion field. We believe that the articles and the selected references to the current literature contained in the articles will prove useful and stimulating.

339 pp., 6 × 9 illus., including one four-color plate, $20.00 Mem., $35.00 List

TO ORDER WRITE: Publications Dept., AIAA, 1290 Avenue of the Americas, New York, N.Y. 10019